RSC Advances

PAPER

View Article Online
View Journal | View Issue

Cite this: *RSC Adv.*, 2023, **13**, 9678

Promising transition metal decorated borophene catalyst for water splitting†

Rongzhi Wang [a] and Jin-Cheng Zheng *[ab]

Received 15th January 2023
Accepted 2nd March 2023

DOI: 10.1039/d3ra00299c

rsc.li/rsc-advances

Borophene has been recently reported to be a promising catalyst for water splitting. However, as a newly synthesized two-dimensional material, there are several issues that remain to be explored. In the present study, we investigate the catalytic performance of three kinds of pristine and decorated borophenes using first-principles calculations. Our calculations show that Ni-doped α borophene can be a highly active catalyst for water splitting. Doping or decorating with different transition metals such as Co or Ni at different sites shows a strong effect on the catalytic performance of α, β_{12} and χ_3 borophenes. Ni-doped α borophene shows low Gibbs free energy of hydrogen adsorption ($\Delta G_H \sim 0.055$ eV) for the hydrogen evolution reaction (HER) and promising overpotential (0.455 V) for the oxygen evolution reaction (OER). This study provides some critical insights into the catalytic activity of borophene for water splitting by selecting suitable decorated metal.

Introduction

The serious environmental and energy crises all over the world have greatly stimulated research interests in the exploration of sustainable energy sources.[1–10] Water splitting is one of the clean and renewable energy technology, and the efficiency of this mainly depends on the performance of the catalysts. To date, the most effective catalysts are Pt (for HER) and IrO_2/RuO_2 (for OER).[11–14] However, the scarcity and high prices prevent their large-scale usage. Therefore, developing cheaper and more effective catalysts for water splitting is extremely needed.

On account of the special physical and chemical properties and the large specific area, two-dimensional (2D) materials have been highly attractive in the past few years. Besides MoS_2, which is a highly effective 2D catalyst comparable with Pt for HER, a new 2D material, borophene, has been reported to be a highly intrinsic catalyst recently.[15] A 2D boron sheet, borophene, which was theoretically predicted and first prepared on Ag (111) in 2015,[16] has many excellent physical properties, such as high strength comparable to graphene[17,18] and super-conductivity.[19,20] In addition, borophene has a substantial number of allotropes such as α, β_{12} and χ_3 phases.[21] According to recent studies,[15,22] borophene also has the possibility of being used as a novel HER catalyst. As borophene is the lightest 2D material, it may become the lightest catalyst for HER. Liu *et al.*[23] reported that boron nanosheets were excellent conductors, metal-free, and could be synthesized readily; they are promising candidates for HER. Shi *et al.*[24] proposed that borophene is a high-performance catalyst for HER with near zero free energy for hydrogen adsorption, metallic conductivity, and plenty of active sites in the basal plane. Tai *et al.*[25] prepared borophene nanosheets on a carbon cloth surface by chemical vapor deposition and found that borophene showed good electrocatalytic HER ability with a 69 mV dec^{-1} Tafel slope and good cycling stability in a 0.5 M H_2SO_4 solution. Zhang *et al.*[26] reported that Au and Ni two-dimensional boron sheets might serve as HER catalysts that were competitive with Pt. Moreover, the HER activity of borophene can be further improved by some methodologies, such as doping some metal elements and strain engineering. Mir *et al.*[27] investigated the influence of the dopants on the catalytic activity of the α phase of borophene sheets and reported that the intrinsic HER catalytic activity of borophene was improved by the doped atoms. Wang *et al.*[28] found that strain engineering was demonstrated to be an effective way to improve the HER catalytic performance of armchair borophene nanoribbons, and free energy of almost zero was achieved at a critical compressive strain of −2%. Subsequently, borophene showed vast application prospects in OER. Singh *et al.*[29] proposed that borophene-supported single transition metal atoms showed high catalytic performance in OER and oxygen reduction reaction (ORR). Xu *et al.*[30] studied the borophene-supported single transition metal atoms as potential OER electrocatalysts using density functional theory calculations and revealed that the Ni atom was useful to enhance the catalytic behavior of borophenes for water splitting. Xu *et al.*[31] designed single-atom bifunctional electrocatalysts for overall water splitting that involved 3d transition metal atom-doped borophene nanosheets. Besides, Erakulan

[a]*Department of Physics, Fujian Provincial Key Laboratory of Theoretical and Computational Chemistry, Xiamen University, Xiamen 361005, China. E-mail: jczheng@xmu.edu.cn*

[b]*Department of Physics and Department of New Energy Science and Engineering, Xiamen University Malaysia, Sepang 43900, Malaysia*

† Electronic supplementary information (ESI) available. See DOI: https://doi.org/10.1039/d3ra00299c

et al.[32] studied that doping nonmetal carbon atoms into borophene could reduce the σ electrons of the adjacent boron atoms making them less reactive towards O* intermediate, and dual carbon doping made β_{12} borophene more efficient towards OER. Moreover, a few groups have demonstrated the introduction of an additional transition metal atom on the δ_3 sheet borophene monolayer,[33] and the β_{12} sheet borophene monolayer[34] can display good electrocatalytic performance. Although there exist several studies on the application of borophene in water splitting illustrated above, the systematic studies on HER/OER catalytic activity of various borophenes are inadequate and the main factors that may affect their HER/OER performance are still unclear, calling for more theoretical studies at the atomic level.

In this work, we rationally adopted two different doping methods, B_{Co}-doping (Co atom substitutes inert B catalytic site) and Ni-doping (Ni atom adsorbs on vacancy site), to study α, β_{12} and χ_3 borophenes for their HER and OER performance by first-principles calculations. With good structural stability and metallic conductivity, Ni-doped borophenes can be used as bifunctional HER/OER catalysts. In particular, Ni-doped α borophene shows the optimal catalytic performance for water splitting.

Computational methods

The first-principles calculations were performed based on the density functional theory, implemented in the Vienna *Ab initio* Simulation Package (VASP).[35] The projector-augmented wave (PAW) pseudopotential[36] was used and the generalized gradient approximation of the Perdew–Burke–Ernzerhof (PBE-GGA) method[37] was employed in the calculations. A 380 eV cut-off energy was set for the plane-wave basis set. The convergence accuracy for the energy was set to 10^{-4} eV and the force converged to 0.01 eV $Å^{-1}$. A 3 × 3 × 1 Monkhorst–Pack *k*-mesh in the Brillouin zone was used for the borophene structure relaxation. The calculations were completed on the 2 × 2 × 1, 3 × 2 × 1, and 3 × 2 × 1 supercells consisting of 32, 30, and 30 boron atoms in α-sheet, β_{12}-sheet and χ_3-sheet, respectively. The doping ratios of the transition metal in these sheets were 1/32, 1/30, and 1/30, respectively. Both the directions perpendicular to the periodic direction have a vacuum of 15 Å to avoid the interaction between neighboring units.

The Gibbs free energy of hydrogen adsorption (ΔG_H) was calculated to evaluate the catalytic activity of borophenes for HER. The free energy ΔG_H is defined as $\Delta G_H = \Delta E_H + \Delta E_{ZPE} - T\Delta S_H$, where ΔE_H, ΔE_{ZPE}, and ΔS_H are the hydrogen adsorption energy, the zero point energy (ZPE), and the entropy differences between the adsorbed state and the gas phase, respectively. The calculation method of ΔG_H used in the present work has been validated in a previous study.[38] Thus, the formula can be rewritten as $\Delta G_H = \Delta E_H + 0.24$. In addition, the adsorption energy per H atom (ΔE_H) is defined as $\Delta E_H = E_{slab+H} - E_{slab} - 1/2E_{H_2}$, where E_{slab+H} and E_{slab} are the total energies of borophenes with and without the adsorbed H atom, and E_{H_2} is the total energy of H_2 gas.

The pathway of OER has been summarized in detail as shown below. In the acid electrolyte, OER can be decomposed into the following elementary steps:

$$H_2O(l) + * \rightarrow OH^* + H^+ + e^- \quad (1)$$

$$OH^* \rightarrow O^* + H^+ + e^- \quad (2)$$

$$O^* + H_2O(l) \rightarrow OOH^* + H^+ + e^- \quad (3)$$

$$OOH^* \rightarrow * + O_2(g) + H^+ + e^- \quad (4)$$

where * represents the active site on the surfaces of the catalysts, l, and g represent the liquid phase and the gas phase, respectively.

For each elementary step of OER, the free energy has been calculated according to the method proposed by Nørskov *et al.*[12] The free energy change from the initial state to the final state of the reaction is defined as:

$$\Delta G = \Delta E + \Delta E_{ZPE} - T\Delta S + \Delta G_U + \Delta G_{pH} \quad (5)$$

where ΔE, ΔE_{ZPE}, and ΔS are the differences in the total energy obtained from DFT calculations, zero point energy, and entropy between the reactants and the products, respectively. T represents the temperature (298.15 K). $\Delta G_U = -neU$, where U is the applied electrode potential, e is the charge transferred and n is the number of proton-electron transferred pairs. In addition, $\Delta G_{pH} = -k_B T \ln[H^+] = pH \times k_B T \ln 10$, where k_B is the Boltzmann constant.

The free energy change for the four elementary OER steps can be obtained as $\Delta G_1 = \Delta G_{OH^*}$, $\Delta G_2 = \Delta G_{O^*} - \Delta G_{OH^*}$, $\Delta G_3 = \Delta G_{OOH^*} - \Delta G_{O^*}$, and $\Delta G_4 = 4.92 - \Delta G_{OOH^*}$. Therefore, the overpotential that evaluates the performance of OER is applied according to the following equation:

$$\eta^{OER} = \max\{\Delta G_1, \Delta G_2, \Delta G_3, \Delta G_4\}/e - 1.23 \quad (6)$$

where 1.23 V represents the equilibrium potential.[11]

The adsorption energies of intermediates OH*, O*, and OOH* are defined as follows:

$$\Delta E_{OH} = E(OH^*) - E(^*) - [E(H_2O) - 1/2\ E(H_2)] \quad (7)$$

$$\Delta E_O = E(O^*) - E(^*) - [E(H_2O) - E(H_2)] \quad (8)$$

$$\Delta E_{OOH} = E(OOH^*) - E(^*) - [2E(H_2O) - 3/2E(H_2)] \quad (9)$$

$E(OH^*)$, $E(O^*)$, and $E(OOH^*)$ are the absolute energies computed for slabs with OH, O, and OOH adsorbed, respectively. $E(^*)$, $E(H_2O)$, and $E(H_2)$ are the energies of the bare slab, H_2O, and H_2 molecules.

The charge density difference (ρ_{diff}) on the borophene before and after the deposition of Ni is calculated:

$$\rho_{diff} = \rho(Ni@borophene) - \rho(borophene) - \rho(Ni) \quad (10)$$

where ρ(Ni@borophene), ρ(borophene) and ρ(Ni) are the charge densities of Ni@borophene, borophene and Ni, respectively.

The adsorption energy (E_a), which is the required energy to dissociate the Ni adatom from the boron sheet and move it away from the sheet, was determined to assess the stability of the Ni-doped system with eqn (8).

$$E_a = E_{B(Ni)} - E_B - E_{Ni} \quad (11)$$

where $E_{B(Ni)}$ and E_B refer to the total energy of Ni-doped borophene and borophene, and E_{Ni} is the energy of the isolated Ni atom.

In our simulation, the formation energy of the Co-substituted B was calculated by the following formula:

$$E_F = E(B_{Co}) - E_B + \mu_B - \mu_{Co} \quad (12)$$

where $E(B_{Co})$ is the total energy of B_{Co}-doped borophene, E_B is the total energy of borophene, μ_B, and μ_{Co} are the chemical potentials of isolated B and Co atoms, respectively.

The climbing image nudge elastic band (CI-NEB) method[39] was performed to investigate the water dissociation on the different surfaces. To be specific, we first deposited an H_2O molecule on the catalyst surface and allowed it to relax to the most stable site. After that, we started with multiple initial configurations and selected the one with the minimum energy. Then, we found the corresponding potential final locations of H^+ and OH^- on the surface and allowed each of these configurations to relax. Finally, we performed CI-NEB calculations on the most stable final H + OH configuration with the most stable initial H_2O configuration.

Results and discussion

The active sites and HER activity of the pristine borophenes

It is well-known that the HER catalytic activity of electrocatalysts highly depends on the H adsorption-free energy (ΔG_H).[40] Generally, the HER catalytic activity is considered to be high if $|\Delta G_H| < 0.2$ eV.[41,42] The closer value of $|\Delta G_H|$ is to 0, the HER catalytic activity is higher.[43] We first studied the HER performance of three typical pristine borophene allotropes, namely, αB, β_{12}B, and χ_3B. Among many predicted structures, αB was confirmed to be the most stable structure,[44] β_{12}B and χ_3B can be synthesized experimentally.[45] These three allotropes have a typical porous characteristic structure that can provide sufficient surface space and active atoms, which are beneficial to be used in the field of catalysis. As shown in Fig. 1, For αB, there are two H adsorption sites namely, αB-S1 and αB-S2. The calculated free energies of the H adsorption at these sites are −0.005 and −0.75 eV, respectively. Thus, HER at αB-S1 site presents high activity as the H adsorption free energy at this site is better than that of Pt (−0.09 eV (ref. 46)), and the very negative free energy of the αB-S2 site shows that the strong H adsorption, which will poison the active site. For β_{12}B, three distinct sites for H adsorption are obtained, β_{12}B-S1, β_{12}B-S2, and β_{12}B-S3. However, the free energies of these sites are very positive which indicates weak H adsorption and HER performance, and the H adsorption free energies of these corresponding sites are 0.253, 0.218, and 0.99 eV, respectively. As for χ_3B, we find two no-equivalent kinds of sites, χ_3B-S1 and χ_3B-S2. The free energy of χ_3B-S1 is 0.031 eV and so this site performs good HER activity than χ_3B-S2 whose free energy is 0.544 eV. In addition, all H atoms adsorb on the top sites of B atoms (see Fig. S1†), and interestingly, all these sites can be classified into three kinds of coordination numbers of B sites, which are 4, 5, and 6 coordinations, as shown in Fig. 1.

The stability of B_{Co}- and Ni-doped borophenes

Next, we adopt two different doping methods, B_{Co}- and Ni-doping, to the aforementioned three kinds of borophenes, *i.e.*, αB, β_{12}B and χ_3B, then to investigate their atomic structures, electronic properties, HER and OER performance. Fig. 2a shows the B_{Co}- and Ni-doped borophene structures. Obviously, B_{Co}-doping barely causes structural distortions to different phases of borophenes. Here the calculated formation energies of B_{Co}-doping into αB, β_{12}B and χ_3B are only 0.663, 0.897, and 0.974 eV, respectively, indicating that the dopant should be relatively easily doped on the surface. On the other hand, we use the Co atom to substitute the inert B catalytic site for HER in different borophene surfaces. For Ni-doping, it can show various degrees of structural distortions to borophenes and distortion degrees obey the sequence of αB < β_{12}B < χ_3B. Ni tends to adsorb on the vacancy site for αB, as shown in Fig. S2,† there are three Ni adsorption sites and the Ni adsorption energy is the highest (−5.218 eV) when it stays on the vacancy site. According to the preceding result, we study the Ni adsorption energies for corresponding vacancy sites on β_{12}B and χ_3B, which are −5.404 eV and −5.149 eV, respectively. These large negative values of Ni adsorption energies on the vacancy sites manifest the high stability of Ni-doped structures. Interestingly, the reason we chose the Co atom to substitute the B atom in our studied structures is shown in Fig. 2b, besides V ($1.752\mu_B$), Cr ($2.975\mu_B$), Mn ($-0.003\mu_B$), and Fe ($-1.611\mu_B$) dopants, other transition metal atoms can keep αB with zero magnetic moments, reflecting the nonmagnetic intrinsic property of αB. Based on zero magnetic moments, B_{Co}-doped αB has the lowest energy. Therefore, Co-substituted B was adopted in our research.

The HER activity and electronic properties of B_{Co}- and Ni-doped borophenes

From the above discussion, it is concluded that the B_{Co}- and Ni-doped borophene structures showcase high stability. The following step is that we explore the HER catalytic abilities of these modified borophene surfaces in detail (see Fig. S3 and S4†). Firstly, it is clear that B_{Co}-doping could bring Co and Co–B bridge new sites for H adsorption toward αB, β_{12}B, and χ_3B. Ni-doping could introduce new Ni sites for H adsorption toward αB and β_{12}B, especially, Ni-doped χ_3B possesses Ni and Ni–B bridge new sites. Secondly, Co new sites perform excellent HER catalytic activities on B_{Co}-doped β_{12}B and χ_3B as a result of near-zero hydrogen adsorption-free energies. Therefore, B_{Co}-doped β_{12}B and χ_3B may be used as highly active single-atom catalysts for HER. Thirdly, new Ni sites of different Ni-doped borophenes

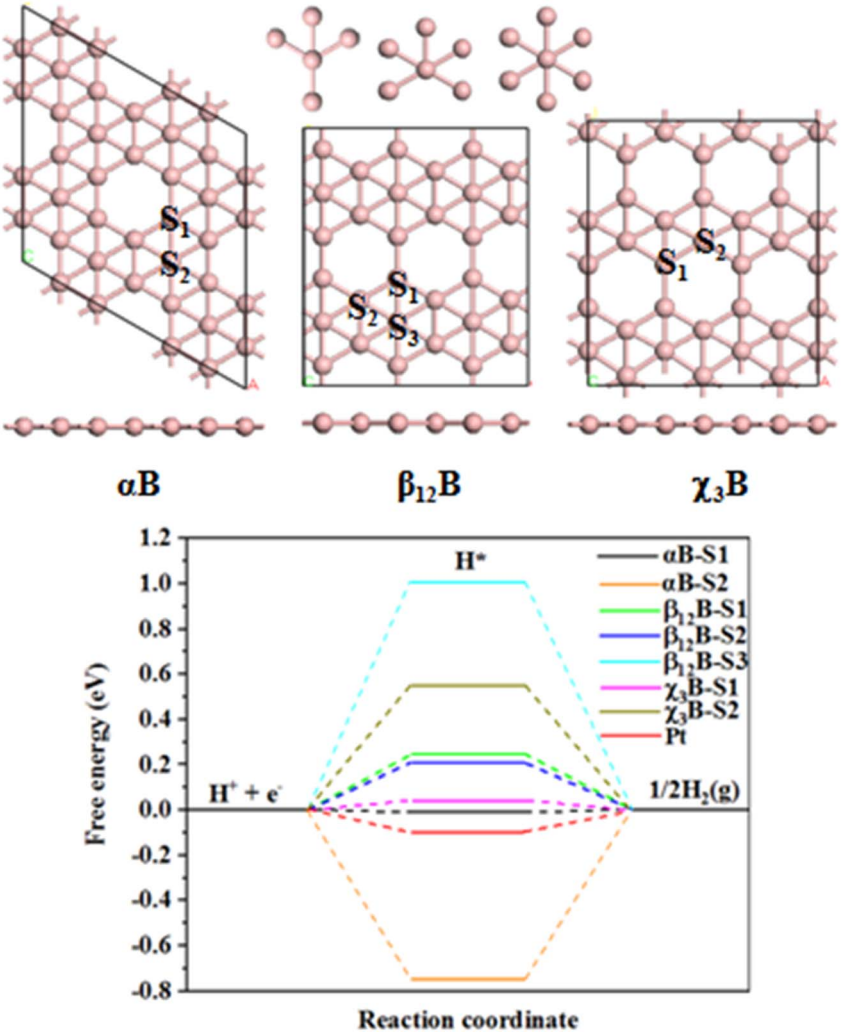

Fig. 1 Models and calculated HER performance: top and side views of atomic structures of αB, β_{12}B, and χ_3B, and calculated the free energy diagram for HER of different sites in various borophenes and cited data.

showed inferior HER performance along with very positive hydrogen adsorption-free energies.

Then, as far as the best active sites of B_{Co}- and Ni-doped surfaces for HER are concerned, as shown in Fig. 3, from three free energy diagrams for hydrogen evolution, it is clear that B_{Co}- and Ni-doping are effective to modulate the HER performance of αB, β_{12}B, and χ_3B. Specifically, for B_{Co}-doping, the hydrogen adsorption-free energies of three kinds of borophenes decrease to −0.336, −0.074, and −0.005 eV, respectively. Thus, B_{Co}-doped β_{12}B, and χ_3B behave excellent HER activity as a result of zero approached free energies. Although B_{Co}-doping is not beneficial to improve the HER catalytic activity of αB when pH = 0, B_{Co}-doped αB possesses rich and excellent HER active sites when pH = 7 (see Fig. S5†) and all the active sites on this surface have near zero hydrogen adsorption free energies. Besides, we studied the water dissociation on this surface and find that the energy barrier (0.674 eV) for water dissociation was extremely low (see Fig. S6†); H_2O molecules adsorb on the top site of Co atom and the dissociated H* adsorbs on the bridge site between the Co atom and the nearest neighbor B atom. Considering a relatively high energy barrier of 0.89 eV for the water dissociation on the Pt surface,[38,46] B_{Co}-doped αB shows superior neutral HER catalytic performance, which increases the feasibility of the splitting seawater, the most abundant water source, in H_2 production. The reason is that electrolysers operating in neutral media can potentially enable the direct use of saltwater without the requirement of desalination for pH maintenance.[47] For Ni-doping, the hydrogen adsorption free energies of different modified surfaces are 0.055, 0.176, and 0.13 eV, respectively, implying that Ni-doped αB, β_{12}B, and χ_3B have good HER activity.

We will employ the electronic properties of these pristine and decorated borophenes to enrich the physics insight. Compared to the pristine surfaces, the free energies of the modified surfaces work in small increments or decrements. Furthermore, by analyzing the density of states (DOS) of the pristine, B_{Co}- and Ni-doped borophene surfaces, firstly, these surfaces are metallic as a result of DOS profiles crossing the

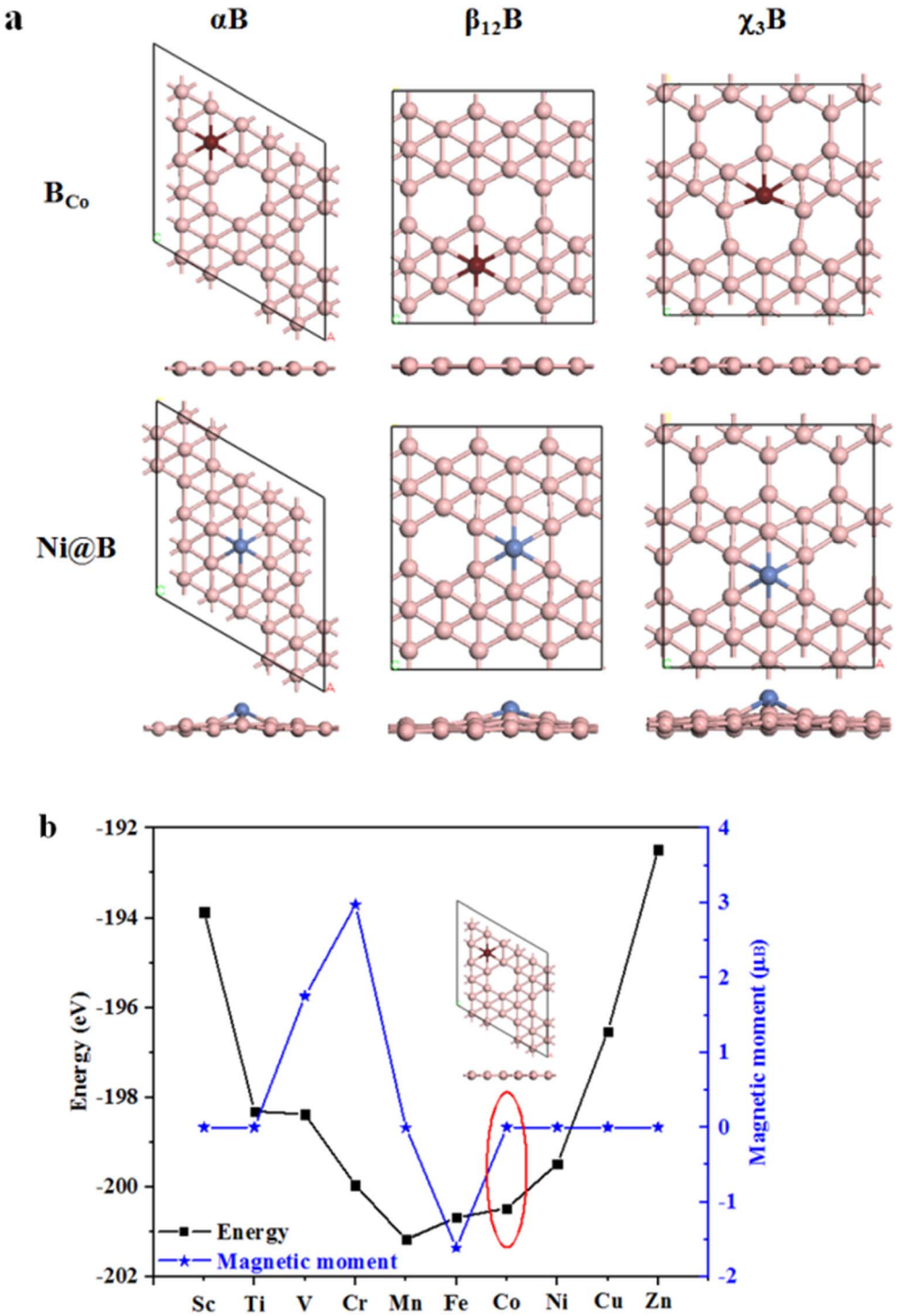

Fig. 2 (a) Top and side views of B_{Co}- and Ni-doped structures; (b) summarized energies and magnetic moments of different metal dopant substitute B in αB. The pink, brown, and blue balls represent B, Co, and Ni atoms, respectively.

Fermi level with no gap. Next, we noticed that B_{Co}-doping leads to the peak values of αB and $\beta_{12}B$ near the Fermi level becoming bigger, however, the peak value of χ_3B near the Fermi level declines drastically. Ni-doping makes the peak values of $\beta_{12}B$ and χ_3B near the Fermi level become smaller, and the peak value of αB remains unchanged with the same DOS profile near the Fermi level. All in all, B_{Co}-doping and Ni-doping could arouse the change in electronic properties of αB, $\beta_{12}B$, and χ_3B except Ni-doped αB. We all know that the changed electronic properties may directly affect the electrical conductivity and catalytic ability of materials, then we get different hydrogen adsorption-free energies of the surfaces mentioned above. Additionally, the phenomenon of the unchanged electronic property of Ni-doped αB explains that Ni-doping could keep the

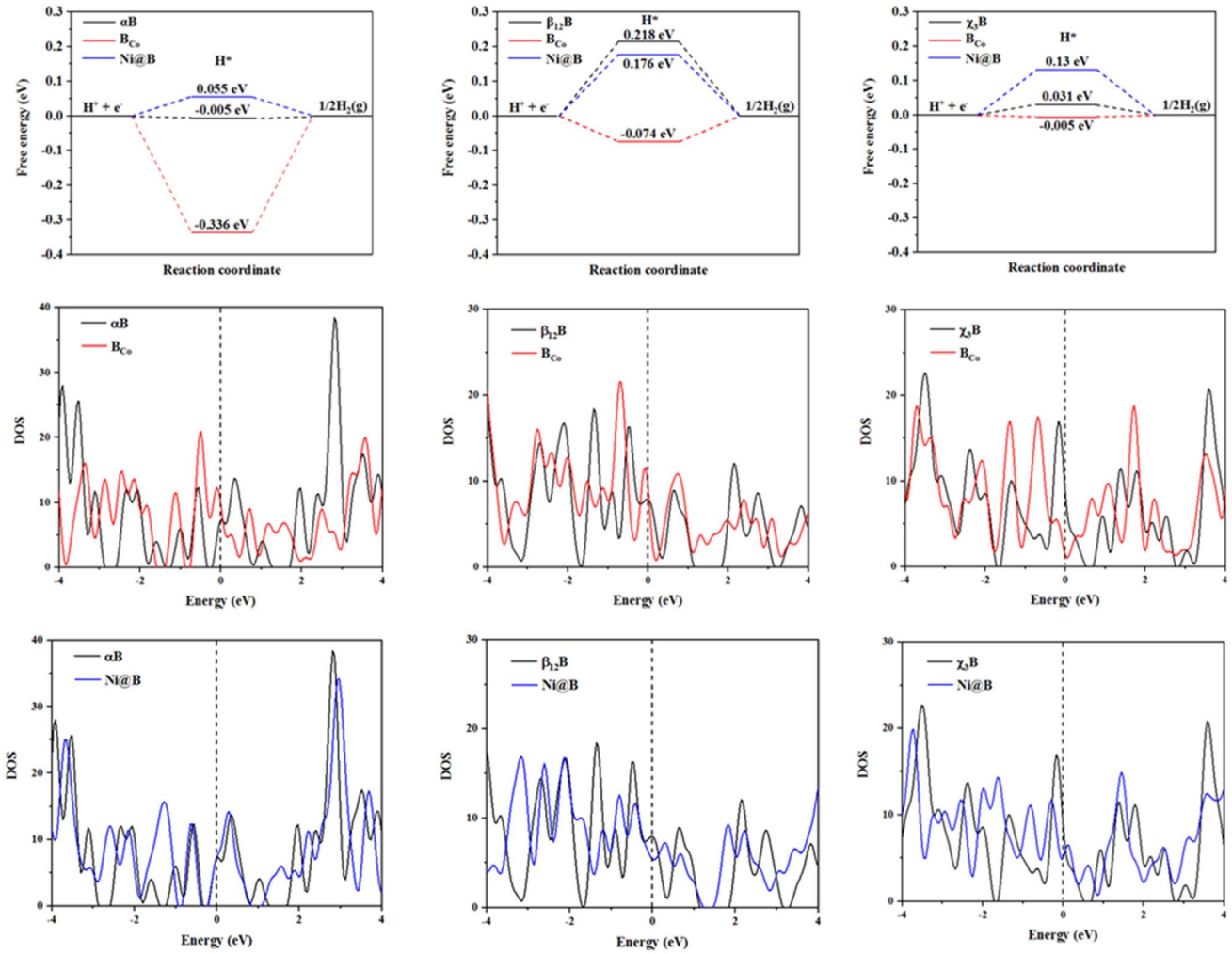

Fig. 3 The hydrogen adsorption free energies of best active sites on pristine, B_{Co}- and Ni-doped borophene (αB, β_{12}B and χ_3B) surfaces; and the DOS of these surfaces, where the Fermi level is set to 0 eV.

stability of αB in the electronic structure, on the other hand, Ni-doped αB maintains the outstanding HER performance from αB.

The OER activity and electronic properties of B_{Co}- and Ni-doped borophenes

After investigating the stability and HER activity of B_{Co}- and Ni-doped borophenes, we study the catalytic activity of these structures for OER. As depicted in Fig. 4a, four elementary steps of OER, Co, and Ni sites are chosen as the active sites for OER, and the structures of the adsorbed intermediates (OH*, O*, and OOH*) on B_{Co}- and Ni-doped borophenes are shown in Fig. S7 and S8.† From the free energy diagram, we can see that for Ni-doped αB, the second step of OH* reacting to O* is the rate-determining step of the entire OER reaction, but for other B_{Co}- and Ni-doped borophenes, the third step of O* reacting with H_2O to form OOH* is the rate-determining step. The reaction Gibbs free energy (ΔG_1, ΔG_2, ΔG_3, and ΔG_4) of the four elementary steps are listed in Table S1.† In addition, we calculated the overpotentials for the corresponding modified borophenes and the overpotential is the most important indicator to determine the OER performance, an ideal OER catalyst is accompanied by zero overpotential.[48] The overpotentials of Ni-doped αB, β_{12}B, and χ_3B are 0.445, 0.498, and 0.543 V, respectively, even lower than that of the state-of-the-art IrO_2 (η^{OER} = 0.56 V (ref. 49)), indicating that the OER catalytic activities of Ni-doped borophenes are better than those of IrO_2. Moreover, B_{Co}-doped borophenes have much bigger overpotentials (η^{OER} = 1.07, 0.804, and 1.113 V, respectively) and lower OER catalytic activities. It is worth noticing that the overpotential for Ni-doped αB is the lowest in this work, implying the best OER performance. Additionally, we plotted the partial density of states (PDOS) analyses of Ni-d orbitals, as shown in Fig. 4b, and find that the lower peak value of Ni-d near the Fermi level means smaller overpotential. Thus, Ni-d of Ni-doped αB manifests the lowest peak value. Apart from Ni-doped αB with different rate-determining steps for OER, we compared Ni-doped β_{12}B with Ni-doped χ_3B combining the PDOS analyses of Ni-d orbitals. The Ni-d peak of Ni-doped χ_3B near the Fermi level within the energy range (−0.5–0 eV) is

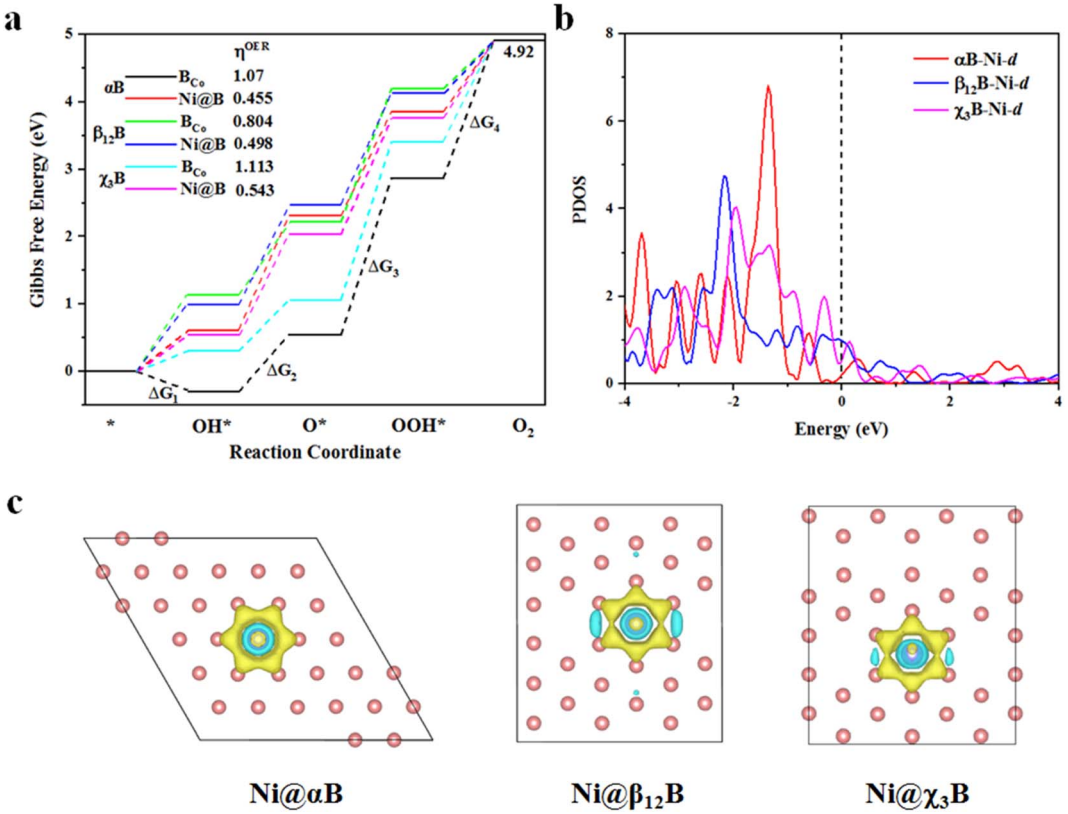

Fig. 4 (a) The Gibbs free energy diagram for the OER pathway of B_{Co}- and Ni-doped borophenes (αB, β_{12}B, and χ_3B); (b) PDOS of Ni-d orbitals in Ni-doped borophenes; (c) charge density differences (isosurface level: 0.008 e Å^{-3}) of Ni-doped borophenes. The yellow and cyan contours represent electron accumulation and depletion, respectively.

higher than that of Ni-doped β_{12}B, indicating that Ni atom of Ni-doped χ_3B has more bonding electrons and then stronger adsorption energy of O*. We obtained the adsorption energies of O* of Ni-doped χ_3B, and β_{12}B as 1.97 eV and 2.45 eV (see Table. S2†), respectively. The stronger adsorption energies of O* will poison the catalytic site and need more potential to form OOH*. Thus, Ni-doped χ_3B has the bigger overpotential.

In general, Ni-doped borophenes show splendid OER catalytic activities and good HER performance from the perspective of extremely low OER overpotentials and Pt-compared hydrogen adsorption-free energies. Also, the charge density differences of Ni-doped borophenes are shown in Fig. 4c, it is visualized to discover that borophenes obtain electrons from Ni atoms and then the electron increase of the borophene systems is beneficial to improve the catalytic activity of catalysts, which may be the inner reason of high water splitting activity of Ni-doped borophenes.

Conclusions

In summary, the catalytic performance of pristine, B_{Co}-and Ni-doped borophenes (αB, β_{12}B, and χ_3B) for HER and OER was systematically investigated using first-principle calculations. Firstly, we examine the HER activities of αB, β_{12}B, and χ_3B, and there exist active sites with hydrogen adsorption-free energies close to zero in αB and χ_3B, indicating that they own excellent HER performance. Then, with good structural stability and metallic conductivity, B_{Co}- and Ni-doping are two effective ways to modulate the HER catalytic activities of different borophenes. B_{Co}-doped αB shows superior neutral HER catalytic performance and B_{Co}-doped β_{12}B and χ_3B could be used as highly active single-atom catalysts for HER. Meanwhile, we studied the OER catalytic activities of B_{Co}- and Ni-doped borophenes in great detail. Ni-doped borophenes showed excellent catalytic abilities for HER and OER; in particular, Ni-doped αB is a promising HER/OER bifunctional electrocatalyst for water splitting with a low hydrogen adsorption free energy (0.055 eV) for HER and overpotential (0.455 V) for OER. Our results indicate that Ni-doped borophenes are expected to be economical and efficient candidates for HER/OER bifunctional electrocatalysts applied to water splitting.

Conflicts of interest

There are no conflicts of interest to declare.

Acknowledgements

This research was supported by the Ministry of Higher Education of Malaysia through the Fundamental Research Grant Scheme (FRGS/1/2021/STG05/XMU/01/1), and the National Natural Science Foundation of China (NSFC) (No. 12274355).

References

1 T. Burger, C. Sempere, B. Roy-Layinde and A. Lenert, *Joule*, 2020, **4**, 1660–1680.
2 I. M. Peters, C. Breyer, S. A. Jaffer, S. Kurtz, T. Reindl, R. Sinton and M. Vetter, *Joule*, 2021, **5**, 1353–1370.
3 J. Janek and W. G. Zeier, *Nat. Energy*, 2016, **1**, 16141.
4 P. Veers, K. Dykes, E. Lantz, *et al.*, *Science*, 2019, **366**, 443.
5 T. Sun, D. Wang, M. V. Mirkin, H. Cheng, J.-C. Zheng, R. M. Richards, F. Lin and H. L. Xin, *Proc. Natl. Acad. Sci. U. S. A.*, 2019, **116**, 11618.
6 G. J. Snyder and E. S. Toberer, *Nat. Mater.*, 2008, **7**, 105–114.
7 J. C. Zheng, *Front. Phys.*, 2008, **3**, 269–279.
8 J. C. Zheng, *Research*, 2022, **2022**, 9867639.
9 L. Han, H. Cheng, W. Liu, *et al.*, *Nat. Mater.*, 2022, **21**, 681.
10 A. Alagumalai, L. Yang, Y. Ding, *et al.*, *Cell Rep. Phys. Sci.*, 2022, **3**, 101007.
11 H. Xu, D. Cheng, D. Cao and X. Zeng, *Nat. Catal.*, 2018, **1**, 339–348.
12 J. K. Nørskov, J. Rossmeisl, A. Logadottir, L. Lindqvist, J. R. Kitchin, T. Bligaard and H. Jonsson, *J. Phys. Chem. B*, 2004, **108**, 17886–17892.
13 T. Reier, M. Oezaslan and P. Strasser, *ACS Catal.*, 2012, **2**, 1765–1772.
14 J. Wang, Y. Fan, S. Qi, W. Li and M. Zhao, *J. Phys. Chem. C*, 2020, **124**, 9350–9359.
15 Z. Wang, T. Lü, H. Wang, Y. Feng and J. C. Zheng, *Front. Phys.*, 2019, **14**, 33403.
16 A. J. Mannix, X. Zhou, B. Kiraly, *et al.*, *Science*, 2015, **350**, 1513–1516.
17 B. Mortazavi, O. Rahaman, A. Dianat and T. Rabczuk, *Phys. Chem. Chem. Phys.*, 2016, **18**, 27405–27413.
18 G. I. Giannopoulos, *Comput. Mater. Sci.*, 2017, **129**, 304–310.
19 X. Zhou, X. Dong, A. R. Oganov, Q. Zhu, Y. Tian and H. Wang, *Phys. Rev. Lett.*, 2014, **112**, 085502.
20 H. Zhong, K. Huang, G. Yu and S. Yuan, *Phys. Rev. B*, 2018, **98**, 054104.
21 X. Sun, X. Liu, J. Yin, J. Yu, Y. Li, Y. Hang, X. Zhou, M. Yu, J. Li, G. Tai and W. Guo, *Adv. Funct. Mater.*, 2017, **27**, 1603300.
22 Y. Chen, G. Yu, W. Chen, Y. Liu, G. Li, P. Zhu, Q. Tao, Q. Li, J. Liu, X. Shen, H. Li, X. Huang, D. Wang, T. Asefa and X. Zou, *J. Am. Chem. Soc.*, 2017, **139**, 12370–12373.
23 C. Liu, Z. Dai, J. Zhang, Y. Jin, D. Li and C. Sun, *J. Phys. Chem. C*, 2018, **122**, 19051.
24 L. Shi, C. Ling, Y. Ouyang and J. Wang, *Nanoscale*, 2017, **9**, 533.
25 G. Tai, M. Xu, C. Hou, R. Liu, X. Liang and Z. Wu, *ACS Appl. Mater. Interfaces*, 2021, **13**, 60987–60994.
26 Z. Zhang, Y. Yang, G. Gao and B. I. Yakobson, *Angew. Chem.*, 2015, **127**, 13214–13218.
27 S. H. Mir, S. Chakraborty, P. C. Jha, J. Wärna, H. Soni, P. K. Jha and R. Ahuja, *Appl. Phys. Lett.*, 2016, **109**, 053903.
28 X. Wang, R. Wu, P. Tian, Y. Yan, Y. Gao and F. Xuan, *J. Phys. Chem. C*, 2021, **125**, 16955–16962.
29 Y. Singh, S. Back and Y. Jung, *Phys. Chem. Chem. Phys.*, 2018, **20**, 21095.
30 X. Xu, R. Si, Y. Dong, L. Li, M. Zhang, X. Wu, J. Zhang, K. Fu, Y. Guo and Y. He, *J. Mol. Model.*, 2021, **27**, 67.
31 M. Xu, X. Zhang, Y. Liu, X. Zhao, Y. Liu, R. Wu and J. Wang, *ChemPhysChem*, 2020, **21**, 2651–2659.
32 E. S. Erakulan and T. Ranjit, *Appl. Surf. Sci.*, 2022, **574**, 151613.
33 A. Banerjee, S. Chakraborty, N. K. Jena and R. Ahuja, *ACS Appl. Energy Mater.*, 2018, **1**, 3571–3576.
34 C. Ling, L. Shi, Y. Ouyang, X. Zeng and J. Wang, *Nano Lett.*, 2017, **17**, 5133–5139.
35 G. Kresse and J. Hafner, *Phys. Rev. B: Condens. Matter Mater. Phys.*, 1993, **47**, 558.
36 G. Kresse and D. Joubert, *Phys. Rev.*, 1999, **59**, 1758.
37 J. P. Perdew, K. Burke and M. Ernzerhof, *Phys. Rev. Lett.*, 1996, **77**, 3865.
38 J. K. Nørskov, T. Bligaard, A. Logadottir, J. R. Kitchin, J. Chen, S. Pandelov and U. Stimming, *J. Electrochem. Soc.*, 2005, **152**, J23–J26.
39 G. Henkelman, B. P. Uberuaga and H. Jónsson, *J. Chem. Phys.*, 2000, **113**, 9901.
40 J. Zhu, L. Hu, P. Zhao, L. Y. S. Lee and K. Wong, *Chem. Rev.*, 2020, **120**, 851–918.
41 Q. Peng, J. Zhou, J. Chen, T. Zhang and Z. Sun, *J. Mater. Chem. A*, 2019, **7**, 26062–26070.
42 G. Gao, A. P. O'Mullane and A. J. Du, *ACS Catal.*, 2017, **7**, 494–500.
43 X. Zhang, A. Chen, Z. Zhang, M. Jiao and Z. Zhou, *J. Mater. Chem. A*, 2018, **6**, 11446–11452.
44 A. R. Oganov, J. Chen, C. Gatti, Y. Ma, Y. Ma, C. W. Glass, Z. Liu, T. Yu, O. O. Kurakevych and V. L. Solozhenko, *Nature*, 2009, **457**, 863–867.
45 B. Feng, J. Zhang, Q. Zhong, W. Li, S. Li, H. Li, P. Cheng, S. Meng, L. Chen and K. Wu, *Nat. Chem.*, 2016, **8**, 563–568.
46 P. Wang, X. Zhang, J. Zhang, S. Wan, S. Guo, G. Lu, J. Yao and X. Huang, *Nat. Commun.*, 2017, **8**, 14580.
47 C.-T. Dinh, A. Jain, F. P. G. de Arquer, P. D. Luna, J. Li, N. Wang, X. Zheng, J. Cai, B. Z. Gregory, O. Voznyy, B. Zhang, M. Liu, D. Sinton, E. J. Crumlin and E. H. Sargent, *Nat. Energy*, 2019, **4**, 107–114.
48 Y. Yang, J. Liu, F. Liu, Z. Wang and D. Wu, *J. Mater. Chem. A*, 2021, **9**, 2438–2447.
49 T. Zhang, B. Zhang, Q. Peng, J. Zhou and Z. Sun, *J. Mater. Chem. A*, 2021, **9**, 433–441.